THE ASTROPHYSICAL JOURNAL, 479:918–925, 1997 April 20

SUPERWIND MODELS FOR THE DUST SHELLS AROUND OH/IR STARS

KYUNG-WON SUH
Department of Astronomy and Space Science, Chungbuk National University, Cheongju-City, 361-763, Republic of Korea; kwsuh@cbucc.chungbuk.ac.kr

AND

TERRY J. JONES
Department of Astronomy, University of Minnesota, 116 Church Street S.E., Minneapolis, MN 55455; tjj@astro.spa.umn.edu
Received 1996 February 16; accepted 1996 November 12

ABSTRACT

We have modeled the dust envelopes around OH/IR stars with the changes in the dust density distribution that are expected from a superwind phase. We explore the effect of a superwind due to a helium shell flash by adding a density-enhanced region that proceeds outward. Depending on the position and the degree of the enhancement, the emergent model spectral energy distributions can be significantly different from the ones with the conventional power-law density distributions. The time evolution of the spectral energy distribution of a superwind can, at certain times, explain some observations of OH/IR stars. However, at other times in the evolution of a superwind, spectral energy distributions and optical depths that are not observed often result.

Subject headings: circumstellar matter — infrared: stars — stars: AGB and post-AGB — stars: mass loss

1. INTRODUCTION

The OH/IR stars are generally considered to be the final phase of an oxygen-rich asymptotic giant branch (AGB) star before leaving the red giant branch and rapidly evolving into a planetary nebula (e.g., Herman & Habing 1985). This phase is characterized by the relatively rapid onset of greatly enhanced mass loss, commonly referred to as the superwind phase (Renzini 1981). As AGB stars evolve, thermal pulses due to internal helium shell flashes have been hypothesized as a major cause of these episodes of greatly enhanced mass loss (Wood 1990). Planetary nebulae often show two, and sometimes three, shell-like structures around them (e.g., Balick et al. 1992). These may be due to abrupt changes in the mass-loss rate back when the star was a dusty AGB (possibly an OH/IR) star, each corresponding to a thermal pulse in the helium-burning shell.

The presence of distinct shells of material around planetary nebulae suggests that these thermal pulse episodes strongly modulate the mass-loss rate from the star. In order to explain the very thick dust shells and high mass-loss rates seen in the more extreme OH/IR stars, the mass-loss rate from an AGB star must increase by at least factor of 10 for the duration of the superwind. We expect one thermal pulse about every 10^4–10^5 yr that endures for a few hundred years (Iben 1975; Vassiladis & Wood 1993). Although the superwind is not expected to be exactly in phase with the thermal pulse, the duration is predicted to be comparable (Vassiladis & Wood 1993).

In this paper, we investigate the influence of a superwind on the emergent spectral energy distribution (SED) of OH/IR stars and similar dusty red giants. We modify the dust density distribution by adding dust to form a region of enhanced density. We then compare our model results with previous model results and the observed SEDs of several OH/IR stars. This is a very different approach than previous modeling of dusty red giants that limited the description of the radial density distribution to power laws with a rather unphysical range in exponents or a simple detached shell.

2. MODEL CALCULATIONS

For this paper, we have used the radiative transfer code of Leung (Egan, Leung, & Spagna 1988). In the present calculations, a radial grid of 125 points and a frequency grid of 70 wavelengths were used. A fixed model parameter for the dust envelope is the wavelength dependence of the dust opacity. The dust condensation temperature (T_c) is assumed to be 1000 K, and the dust condensation radius (R_c) is obtained after a few trials. The outer radius of the dust shell is always taken to be $1000R_c$. The radii of spherical dust grains have been assumed to be 0.1 μm uniformly. The adjustable input parameters are the dust optical depth at 9.7 μm ($\tau_{9.7}$) and the radial dust density distribution. First-order anisotropic scattering is considered for all the models except for a few models with exceptionally high optical depths ($\tau_{9.7} > 60$). For these models, the scattering is not considered because pure absorption is an adequate description for such thick dust shells.

For the central star, the luminosity is taken to be 1×10^4 $L_\odot$, and a stellar black body temperature of 2000–3000 K is used. A change in the luminosity does not affect the shape of the output spectra; it only affects the overall energy output. A significant change in the blackbody temperature of the central star does affect the output spectra, especially for the models with optically thin dust shells. This is due to the fact that in optically thin dust shells the underlying energy distribution of the star strongly influences the emergent near-infrared continuum.

2.1. *Dust Opacity*

We have obtained a set of optical constants adapting both experimental data and model fitting with observations described in our previous work (Suh, Jones, & Bowen 1990; Suh 1991). For given characteristics of the dust material (the optical constants, the size, and the shape) the absorption and scattering efficiency factors can be calculated at any given wavelength (e.g., Bohren & Huffman 1983). As noted by many authors (e.g., Bedijin 1987; Volk & Kwok 1988; Suh 1991), the wavelength-dependent opacity that fits the

observations best is different for OH/IR stars with optically thin dust shells compared with more dusty stars. The deduced opacities at around 12 μm for optically thick OH/IR dust shells are higher than for optically thin OH/IR dust shells. This may be due to a change in the optical constants as a function of the temperature of the dust grains (Suh 1991). For the optically thick OH/IR stars, the major fraction of the dust grains that contribute to the SED are at cooler temperatures. We have chosen a shell optical depth of $\tau_{9.7} = 3$ to be the dividing line between use of the two opacity laws. Figure 1 shows the absorption and scattering efficiency factors versus wavelength for spherical dust grains with a radius of 0.1 μm. This opacity pattern closely resembles the opacity pattern used by many authors for modeling OH/IR stars with continuous radial density distribution (e.g., Bedijin 1987; Volk & Kwok 1988; Groenewegen 1994).

2.2. *Dust Density Distribution*

Radiative transfer models for AGB stars have been developed by a number of authors with various assumptions on input parameters and differing degrees of sophistication (e.g., Jones & Merrill 1976; Rowan-Robinson & Harris 1983; Bedijin 1987; Volk & Kwok 1988; Suh 1991). These models all assumed a smoothly distributed spherically symmetric dust shell with a power-law description of the radial density distribution. The dust density distribution was most often taken to be inversely proportional to the square of the distance, as would be expected for the constant velocity winds found in OH/IR stars. Werner et al. (1980) and van der Veen et al. (1995) argued that a flatter or steeper density distribution (i.e., $\rho \propto r^{-1}$ or $\rho \propto r^{-3}$) fits better for many dust-thick OH/IR stars (with their choice of opacities). Both simple radiation pressure models (e.g., Kwok 1975; Kozasa, Hasegawa, & Seki 1984) or models that add pulsation and shocks (Bowen 1988; Suh et al. 1990) predict r^{-2} density laws. These models show that dust grains are accelerated relatively fast and approach and maintain terminal velocity within 3–5R_c. Dust formation and growth timescales are very short (about a week) compared with other timescales typical in OH/IR star winds (e.g., Suh et al. 1990). This burstlike grain formation implies a constant outflow velocity for most of the dust shell. The modest departures from constant velocity near R_c found by Suh et al. (1990) have only minor effects on the emergent spectrum.

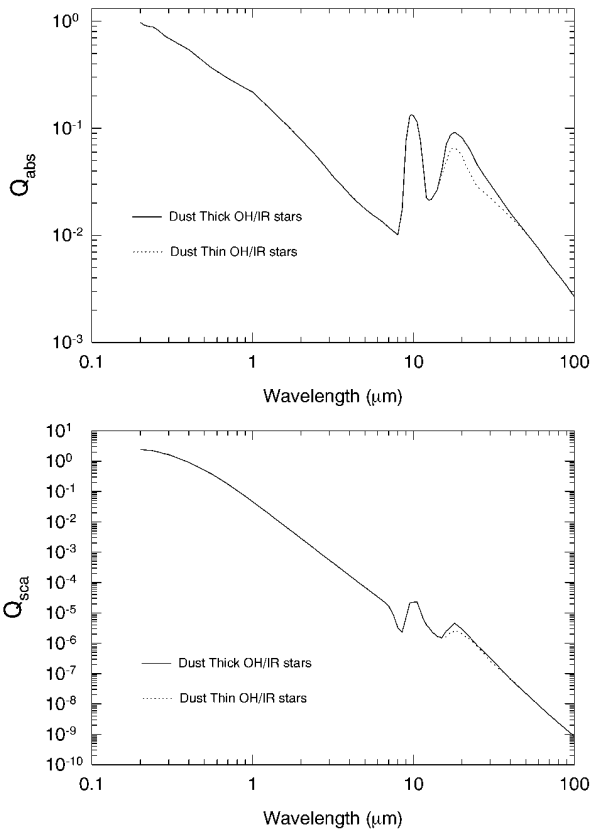

FIG. 1.—Absorption and scattering efficiency factors for the model dust grains.

The dust condensation radius (R_c) is about 2×10^{14} cm for typical OH/IR stars. At a typical expansion velocity of 10–20 km s^{-1}, the lifetime of the thermal pulse ($\sim$500 yr) corresponds to about 2×10^{16} cm, or about 100R_c. Thus, the region of enhanced mass-loss should be about 100R_c thick and travel out from the star with time. Given the expected time between thermal pulses, at most only one region of enhanced density should be within 1000R_c of the star at any one time. The dust distribution in OH/IR stars beyond 1000R_c does not contribute significantly to the infrared spectral energy distribution and therefore has little observable effect until the transition to a planetary nebula. In planetary nebulae, optical images often reveal shells of material far beyond 1000R_c. Frank, van der Veen, & Balick (1994) find that multiple shells are typically separated by approximately (2–30) $\times 10^{17}$ cm, which corresponds to dynamic timescales of (1–15) $\times 10^{4}$ yr, comparable to the theoretical thermal pulse interval (10^{4}–10^{5} yr). The travel time for dust to reach the outer edge of the shell at 1000R_c is about 5000 yr, which is comparable to the interval between thermal pulses on the AGB. Thus, on average, there should at most be only one discontinuity or density enhancement in any OH/IR star shell, but we may expect that a significant fraction of OH/IR stars have a discontinuity in their dust shells if a thermal pulse is the cause of their high mass-loss rates.

If a thermal pulse strongly effects the mass-loss rate from the star, the dust density distribution will be different from a smooth radial distribution. Figure 2 illustrates a description of the hypothesized density discontinuity that we will use in the models. The radial density distribution is still an r^{-2} power law, except for an abrupt elevation of the density in the region of the superwind. The controlling parameters for this enhancement are its inner and outer radii, R_1 and R_2, and the factor by which the density is enhanced over the distribution for the rest of the shell (i.e., 10×, 20×, etc.). Initially, a 10× enhancement of the mass-loss rate will produce a narrow region of enhanced density at the inner boundary of the shell. The leading edge of this enhancement (R_2) will travel out into the shell with time. The radial thickness of the region of enhanced dust shell density will continue to grow until it is 100R_c thick, at which time the superwind stops and the inner edge (R_1) begins to move out in radius as well. The total mass ejected by a thermal pulse is to be conserved; hence, the density falls as r^{-2} as it moves outward. The controlling parameter for any specific shell model, the optical depth at 9.7 μm, is the total line-of-sight optical depth through all portions of the shell.

The actual density law within the enhancement itself may be more complicated than the r^{-2} law in our model (Fig. 2).

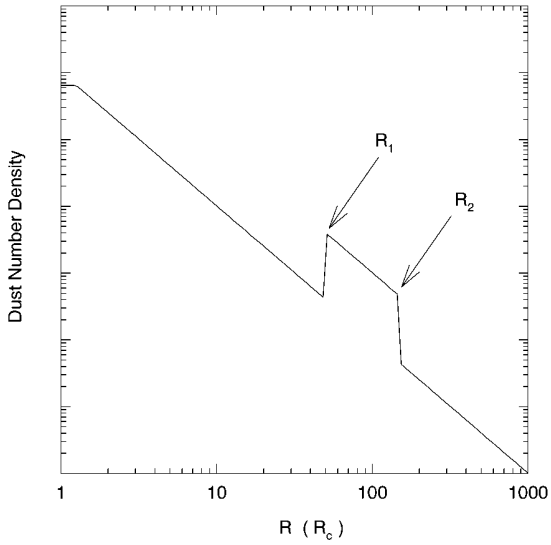

FIG. 2.—The radial form of the dust density enhancement

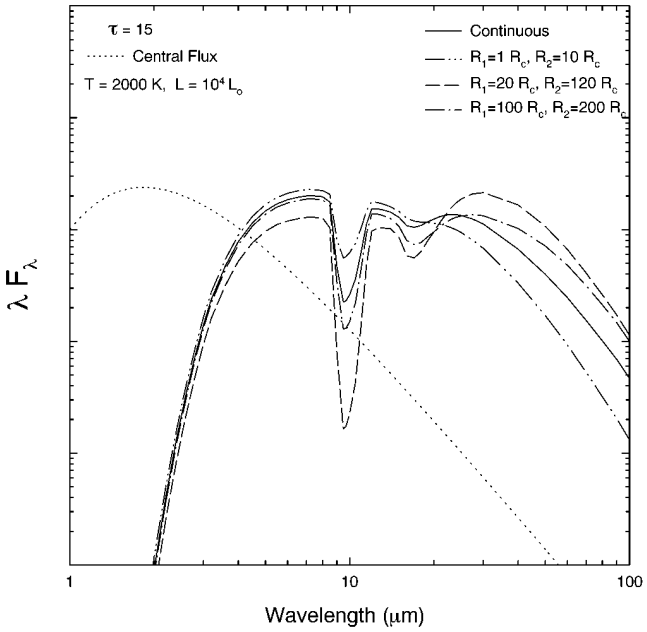

FIG. 3.—Superwind model results with different locations for the discontinuity.

The boundary may not be sharp, and the density within the enhancement may reflect some of the variations seen in hydrodynamic models (e.g., Vassiladis & Wood 1993). We find that our model results are primarily sensitive to the optical depth through the density enhancement and the radial location of the boundaries of the enhancement. Our model spectral energy distributions are largely insensitive to the details of the boundary of the density enhancement or fluctuations in the density law between these boundaries. The density distribution in the superwind enhancement could be predicted with far more detail using sophisticated hydrodynamic models, including shocks, formation and destruction of molecules and dust, etc. But this is beyond the scope of this work.

When such steep density gradients are imposed, there need to be enough radial grid points to achieve rapid convergence for the model and accuracy in flux conservation. If the grid point spacing in the interior of the shell is uniform in log r (as is typical in these models), then the density discontinuity takes place between two adjacent grid points. This produces a temporary departure from constant flux (which must be preserved) at the boundaries of the enhancement. By adding several more grid points between the two original grid points and slightly smoothing the discontinuity, a much smoother average flux distribution can be obtained. That is, the density contrast still takes place over the same physical distance as the simple grid point distribution but can be described in much finer detail at the two discontinuity boundaries. We have tested many different radial grid point distributions and compared the results. Perhaps surprisingly, the different models with the same density enhancement in physical radius give almost the identical outgoing energy spectra, regardless of the detail imposed on the grid point distribution at the discontinuity boundaries. This lends confidence that our models with the sharp discontinuity are physically realistic.

2.3. *General Model Characteristics*

Figure 3 shows the results for a series of models with the same optical depth $\tau_{9.7} = 15$. The conventional model corresponds to a continuous r^{-2} density distribution. For each superwind model, the density enhancement spans a thickness of $100R_c$ (or less if the superwind phase has just started) and has the same density contrast of a factor of 10 at the boundaries of the enhancement. The four superwind models differ only in the radial location of the enhancement in the shell. Note that since all of these models have the same optical depth, the presence of a density enhancement reduces the amount of dust outside the enhancement relative to the continuous model.

If the dust density enhancements begin at $1R_c$ and end at 10–$100R_c$ (very early in a superwind phase), the model SEDs show less flux at far-infrared wavelengths than continuous models. If the density enhancement begins at large radii, the models predict more far-infrared flux than the conventional model. The farther R_1 is from the star, the less the effect of the enhancement on the SED. This is due to the fact that the fraction of the total optical depth to the star contributed by the enhanced density region is progressively smaller as the enhancement approaches the outer edge of the model shell at $1000R_c$. Note that this is a very different model than a detached shell used to model stars making the transition from red giant to planetary nebula (e.g., Volk & Kwok 1989).

The most dramatic departure from continuous models takes place when the inner edge of the density enhancement (R_1) is placed close to the condensation radius within about 10–$30R_c$. The timescale for R_1 to be in this radial regime is only a few percent of the time between thermal pulses. Consequently, the fraction of OH/IR stars with a superwind region in their dust shell that is very close to the inner edge of the shell will be very small, perhaps one in 100. If the hypothesis of a superwind driven by a thermal pulse is correct, the majority of OH/IR stars with density enhancements in their dust shells will have an enhancement that begins at radial distances of $100R_c$ or more.

Figure 4 compares the results of three simple power-law models ($\rho \propto r^{-\beta}$) with $\beta = 1.5$, 2 (the conventional model), and three with our superwind models. Placement of the

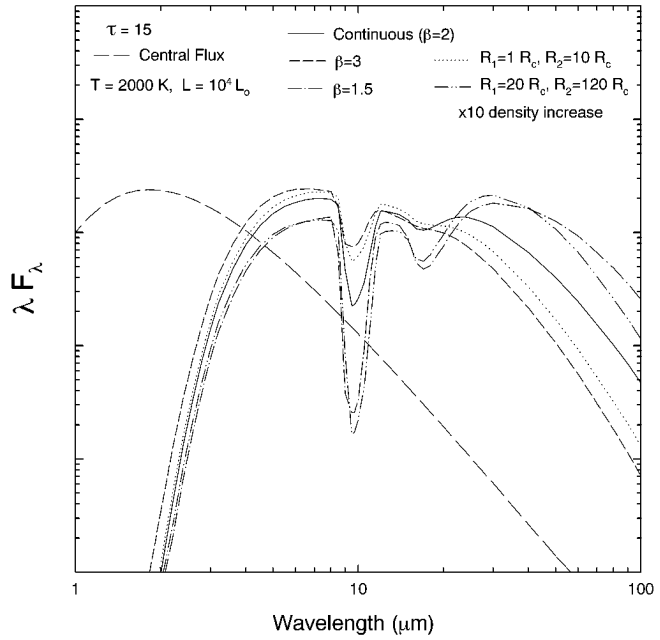

FIG. 4.—Comparison of our superwind models with power-law models

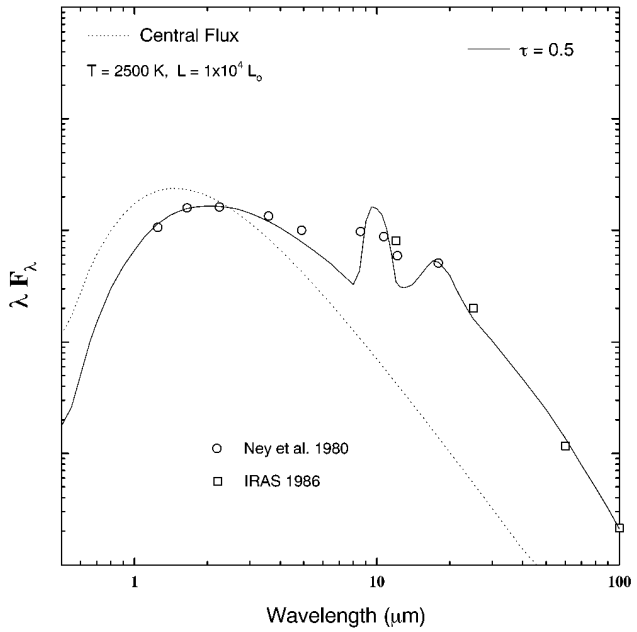

FIG. 5.—Conventional model results compared with observations of IK Tau.

density enhancement at small distances ($R_1 = 1R_c$, $R_2 = 10R_c$) from the star has an effect similar to using a steep r^{-3} density law. Movement of the density enhancement farther ($R_1 = 20R_c$, $R_2 = 120R_c$) from the star has an effect similar to using a more shallow $r^{-1.5}$ density law. Steeper or flatter power-law density distributions are in general not physically plausible. These density laws were explored by previous authors mainly because they fitted the observations better than the r^{-2} law.

3. SPECTRAL ENERGY DISTRIBUTION COMPARISON

For modeling, we have selected five OH/IR stars covering a wide range in optical thickness for the dust shell as representative of our results. These stars are IK Tau, which has a relatively thin dust shell, NV Aur, with a moderately thick dust shell, OH 26.5+0.6 and OH 32.8−0.3, with a very thick dust shell, and OH 21.5+0.5, with an extremely thick dust shell. In all cases the possibility of interstellar absorption has been ignored (but see Jones & Gehrz 1990).

Results of the model calculations (*lines*) superposed on observational data (*symbols*) for IK Tau ($\tau_{9.7} = 1$) and NV Aur ($\tau_{9.7} = 3$) are shown in Figures 5 and 6, respectively. Both are well fitted by a conventional r^{-2} power law for the shell density distribution. Although these stars are considerably dustier than the optically discovered classical Mira variables, they do not have mass-loss rates as high as the very dusty OH/IR stars, such as the radio-luminous OH/IR (RLOH/IR) stars (Jones 1987). It is probable they have not yet had a superwind episode; consequently, they show no evidence of a density enhancement in their SEDs. This does not preclude other OH/IR stars with modest dust shells from having a density enhancement in their shells.

The results of the model calculations (*lines*) superposed on observational data (*symbols*) for the next three stars, OH 26.5+0.6 ($\tau_{9.7} = 15$), OH 32.8−0.3 ($\tau_{9.7} = 15$), and OH 21.5+0.5 ($\tau_{9.7} = 30$), are shown in Figures 7, 8, and 9, respectively. These three stars are examples of the very dusty RLOH/IR stars. Note that the 100 μm fluxes for all three stars and the 60 μm flux for OH 32.8−0.3 are upper limits. These stars have very thick dust shells and will lose a significant fraction of their total mass in the approximately 10^4 yr they spend as RLOH/IR stars. The concept of the superwind was originally developed to explain this class of star, and they are the most likely candidates to have had a superwind phase driven by a thermal pulse. Conventional models provide a reasonable fit to the observations from the near-infrared through the 9.7 μm silicate absorption feature. They do less well at longer wavelengths, and for OH 21.5+0.5 the conventional model does not reproduce the

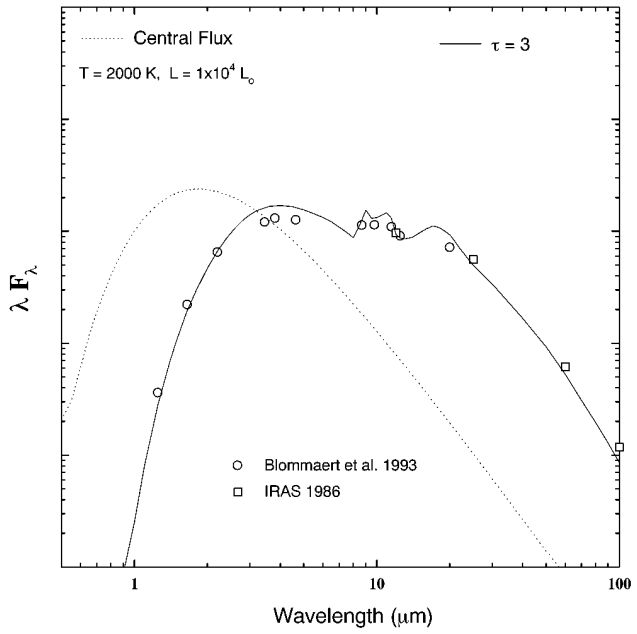

FIG. 6.—Conventional model results compared with observations of NV Aur.

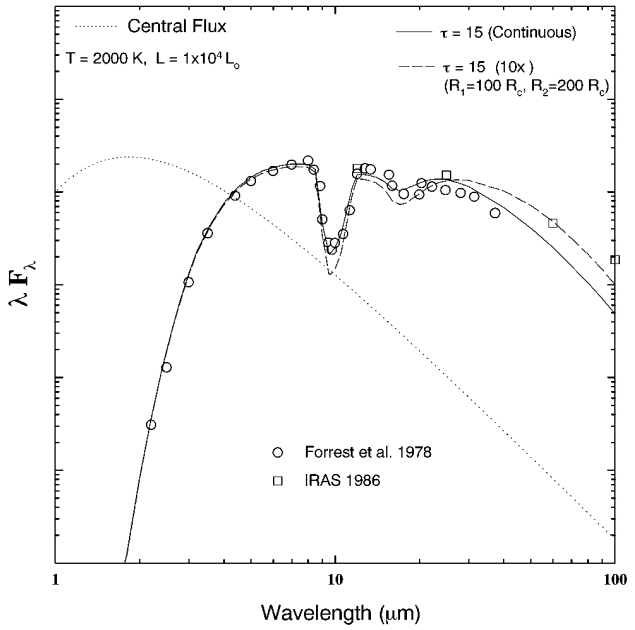

FIG. 7.—Superwind model results compared with observations of OH 26.5+0.6.

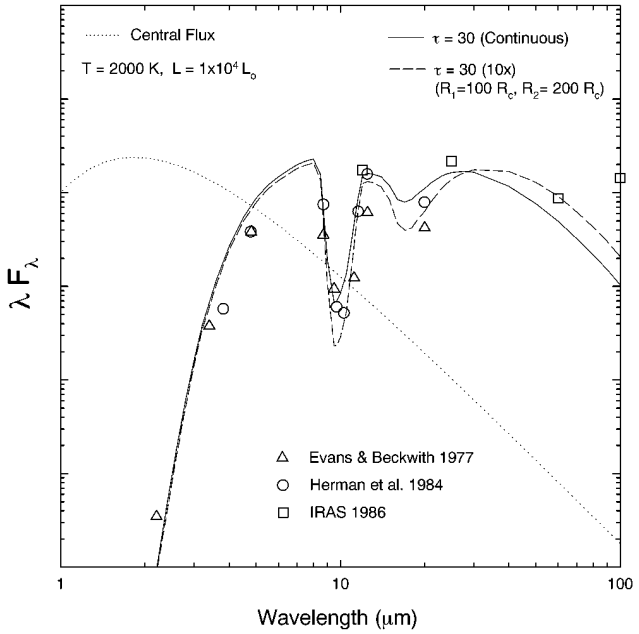

FIG. 9.—Superwind model results compared with observations of OH 21.5+0.5.

depth of the second silicate feature at 18 μm very well. Superwind models with an density enhancement starting at $100R_c$ do a better job of fitting the longer wavelength portion of the SED and do equally well in the near-infrared and at 9.7 μm.

4. COLOR-COLOR DIAGRAMS

Only a relatively small number of OH/IR stars have complete or nearly complete SEDs. *IRAS* four-color photometric data (*IRAS* Point Source Catalog 1986) are available for 758 OH/IR stars (Le Squeren et al. 1992; Blommaert, van der Veen, & Habing 1993; Chengalur et al. 1993; Xiong, Chen, & Gao 1994; Lepine, Ortiz, & Epchtein 1995). Figure 10 plots 475 OH/IR stars in an *IRAS* λF_λ two-color diagram using [60] − [25] versus [25] − [12]. Stars with only upper limits at any wavelength were not used. The small triangles are the observational data, and the lines with large symbols are the model calculations for a range in dust shell optical depth of $\tau_{9.7} = 0.01$–40. In this diagram, differences between the conventional model and the superwind models are more pronounced. By placing a density enhancement at various locations in the dust shell, portions of the diagram that are inaccessible to the conventional models can be covered.

Conventional models cannot extend much beyond the central portions of the diagram, even with very high optical

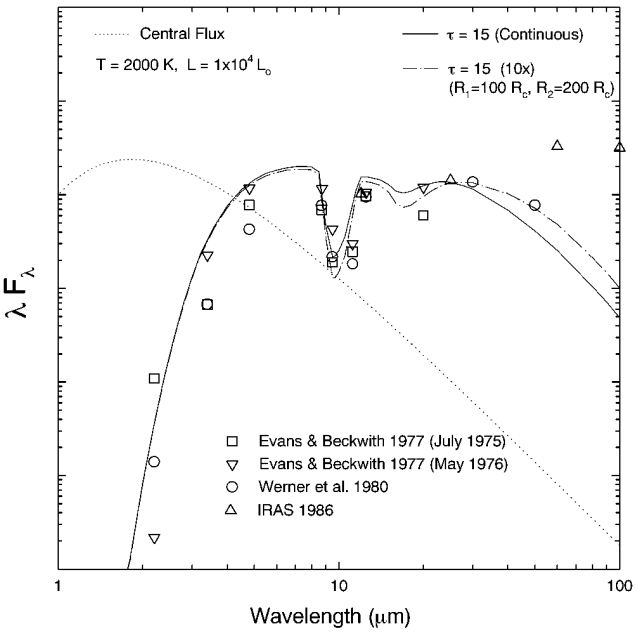

FIG. 8.—Superwind model results compared with observations of OH 32.8−0.3.

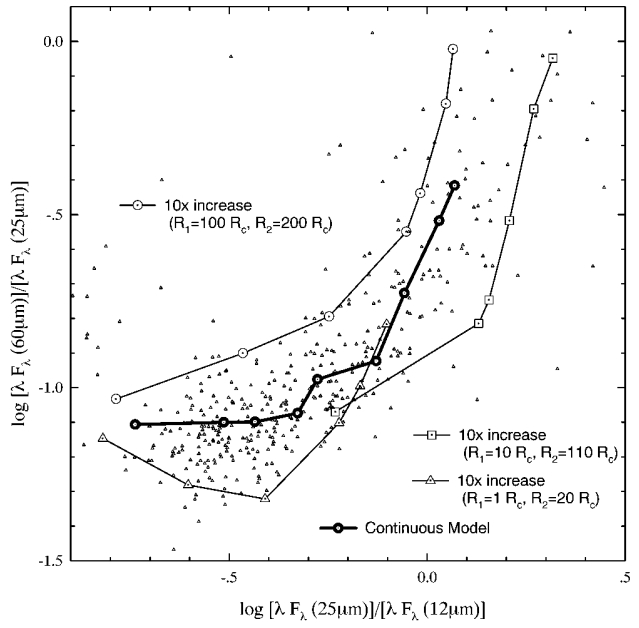

FIG. 10.—Loci of superwind models in the *IRAS* two-color diagram

depths ($\tau_{9.7} = 40$). Superwind models with a distant density enhancement produce redder (cooler) [60] − [25] colors than can be achieved by the conventional model. Even at optical depths as low as $\tau_{9.7} = 0.1$, the superwind model with a 10× density increase beginning at $100R_c$ produces redder [60] − [25] *IRAS* colors. Superwind models with R_1 within 10–$20R_c$ produce colors redder at both [60] − [25] and [25] − [12] for a given optical depth. In general, our superwind models cover a larger portion of the *IRAS* two-color diagram than conventional models alone.

Not all of our superwind models in Figure 10 are consistent with observed near-infrared continua and silicate absorption features. This is true primarily for the model with $R_1 = 10R_c$, which produces a deeper silicate absorption feature than usually observed. Also note that the superwind models with distant density enhancements that reproduce very red colors have significant optical depths for the inner portions of the shell. As mentioned in § 2, when the density enhancement is well away from the condensation radius, most of the optical depth for the shell is at the inner radii. This will have implications for the model evolution of a superwind event if time is wound back until the density enhancement is in the inner positions of the dust shell.

5. TIME EVOLUTION OF THE SPECTRAL ENERGY DISTRIBUTION

If a thermal pulse is the sole cause of the very high mass-loss rates seen in the RLOH/IR phase of the evolution of an AGB star, then the mass-loss rate should return to a lower value when the superwind phase is over. As the superwind enhancement moves out, its density will drop as r^{-2}. Once the superwind stops and the inner edge of the enhancement moves out from the star, the contribution of the enhancement to the total shell optical depth will drop very quickly. The evolution of the optical depth of a dust shell with a superwind is shown in Figure 11 as a function of the position of R_2. The superwind phase has a mass-loss rate 10 times the quiescent phase and lasts long enough (about 500 yr) to produce an enhancement that is $100R_c$ thick.

Immediately apparent in Figure 11 is the fact that the transient superwind model cannot produce high shell optical depths when the outer edge of the density enhancement has moved much beyond $100R_c$. In other words, OH/IR stars with large shell optical depths must presently be losing mass at high mass-loss rates. Any distant enhancement from a previous superwind phase will change the far-infrared colors, but the major fraction of the optical depth must still be due to dust in the inner portions of the shell. Either the star is currently in a second superwind phase because of a thermal pulse, or the overall high mass-loss rate is more ubiquitous and a product of some other mechanism. In this view, the distant enhancement may still be due to a past thermal pulse, but it would be on top of an already high mass-loss wind.

Figure 12 shows the evolution of three superwind models in the *IRAS* two-color diagram. Table 1 lists the change in several physical parameters with time for these models. In each case, the superwind was set to produce a tenfold increase in the mass-loss rate for a time long enough to produce an enhancement $100R_c$ thick. The mass-loss rate then returned to the preceding level as the enhancement moved steadily farther from the star at the terminal wind velocity. The three models are distinguished by a quiescent phase optical depth of $\tau_{9.7} = 0.1$, 3, or 15. Note that the timescale along the model loci is not linear. Evolution in *IRAS* colors is very rapid early in the superwind phase (Fig. 11).

The third model starts with a thick dust shell ($\tau_{9.7} = 15$) already characteristic of a superwind phase and then adds in a 10× superwind. Although this model seems to cover a large portion of the *IRAS* two-color diagram as it evolves, most of the early history of this model produces dust shells with other characteristics that are not observed. Soon after the superwind phase starts, the shell optical depth rapidly approaches a value of $\tau_{9.7} = 150$ and produces a silicate

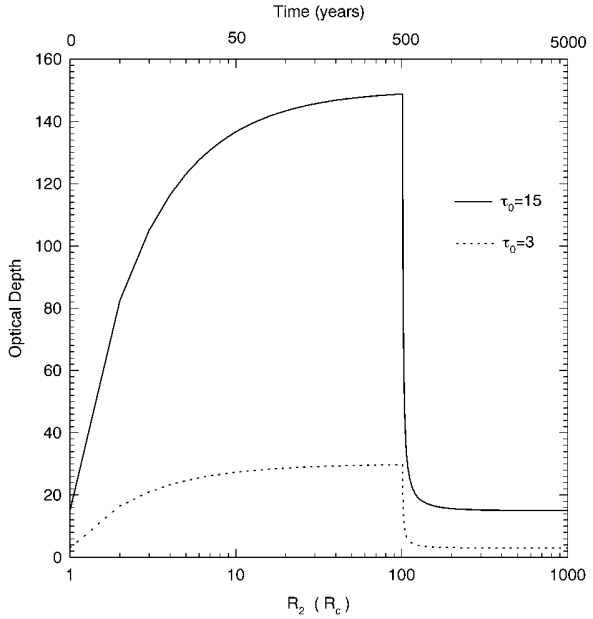

FIG. 11.—Evolution of the total shell optical depth ($\tau_{9.7}$) from the beginning of a superwind phase ($R_2 = R_c$) until the density enhancement reaches $1000R_c$.

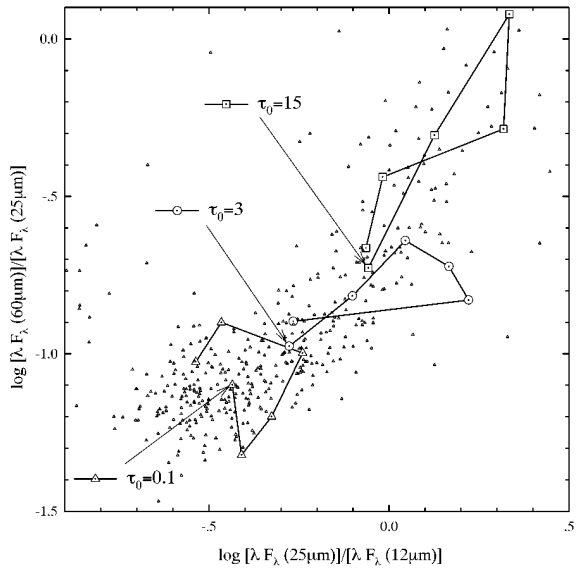

FIG. 12.—Evolution of the colors for three superwind models in the *IRAS* two-color diagram. The arrows point to the *IRAS* colors at the start of the superwind phase. The models extend to approximately 5000 yr after the onset of the superwind.

TABLE 1

TIME EVOLUTION OF OPTICAL DEPTHS AND *IRAS* COLORS

		τ			[25] − [12]			[60] − [25]		
TIME[a]	REGION[b]	$\tau_0 = 0.1$	$\tau_0 = 3$	$\tau_0 = 15$	$\tau_0 = 0.1$	$\tau_0 = 3$	$\tau_0 = 15$	$\tau_0 = 0.1$	$\tau_0 = 3$	$\tau_0 = 15$
0.....	...	0.1	3	15	−0.43	−0.28	−0.057	−1.1	−0.98	−0.72
100.....	1–20	0.91	29	140	−0.41	−0.10	0.13	−1.3	−0.82	−0.31
500.....	1–100	0.99	30	150	−0.33	0.045	0.33	−1.2	−0.64	0.078
600.....	20–120	0.14	4.1	21	−0.24	0.22	0.32	−1.0	−0.83	−0.29
1000.....	100–200	0.1	3.1	16	−0.47	−0.09	−0.017	−0.90	−0.83	−0.44
3000.....	500–600	0.1	3	15	−0.54	−0.27	−0.064	−1.0	−0.90	−0.66

[a] The time (yr) after superwind enters into the inner edge of the dust shell.
[b] The region of the 10× dust density enhancement; $R_1 - R_2$ (R_c).

absorption feature far deeper than observed for any OH/IR star.

6. DISCUSSION

Our dust shell models incorporating a past superwind event fitted the SEDs of some OH/IR stars better than a conventional r^{-2} density distribution. This is particularly the case for the very dusty RLOH/IR stars with excess 30–100 μm emission and deeper 18 μm absorption compared with the conventional model. For these stars, a superwind model with a density enhancement at large distances from the star, 100 or more times the condensation radius, will produce the extra far-infrared emission. It will also improve the model fit in the vicinity of the 18 μm silicate absorption feature. Differences between superwind models and the conventional model are often not very great. In most stars, the best-fit superwind model was nearly identical to the conventional model at most wavelengths.

If we take the superwind model in its simplest form, some problems in interpretation arise. If OH/IR stars have relatively low mass-loss rates between thermal pulses ($<10^{-5}$ $M_\odot$ yr^{-1}), then mass-loss rates a factor of 10 or more higher ($>10^{-5}$ $M_\odot$ yr^{-1}) will take place only during the superwind phase. In the early stages of the superwind, in which the density enhancement is just beginning to travel into the dust shell, the model SEDs do not resemble the SEDs of typical OH/IR stars. This is a very short period of time ($\sim$100 yr) and may be too rare to be observed in a significant number of sources. Well into the superwind phase, but before the superwind stops, the models closely resemble conventional models. This is expected, since the superwind density enhancement is $100R_c$ thick, and if it extends from 1–$100R_c$, it closely mimics a conventional model.

For the very dusty OH/IR stars that are well fitted by a superwind model with a distant density enhancement, their large optical depths are indicative of an ongoing superwind. In other words, the density enhancement would have to be on top of what already amounts to a very high mass-loss wind. This would make the effects of a thermal pulse something of a "super superwind" and suggests some other underlying mechanism for the formation of the very thick OH/IR star dust shells. Unfortunately, the evolution of the SED of a star with a superwind phase on top of a very high quiescent mass-loss rate passes through several phases that are not observed in any known OH/IR star. For example, if the quiescent optical depth is $\tau_{9.7} = 10$, then as the superwind phase progresses, the optical depth increases to a value of approximately 100 within a few hundred years. These extreme optical depths are not observed. Soon thereafter, the superwind stops and the optical depth of the dust shell very rapidly returns to the quiescent optical depth, but now with density enhancement well out into the shell.

This later phase, which lasts for several thousand years, best represents the superwind models that match the SEDs of the RLOH/IR stars. This phase lasts for about 90% of the duration of the superwind event (i.e., out to $1000R_c$). It is possible that we have missed the RLOH/IR stars that are in the first few hundred years of a superwind event, when the shell structure is so peculiar. First, not all RLOH/IR stars would necessarily have a superwind event located within $1000R_c$. Second, less than one in 10 of those that do would be in the early phase with a very peculiar density distribution. Moreover, if optical depths of $\tau_{9.7} = 100$ or more are actually achieved, then the star may be completely invisible at all but far-infrared wavelengths for much of this early phase.

In addition to theoretical predictions of transient high mass-loss winds as a result of a thermal pulse, the observations of shells around planetary nebulae were another major motivation for developing our superwind models. According to our results, the effect of the superwind are probably more prominent in the planetary nebula stage, in which past enhancements to the mass-loss rate are shocked from the inside by the fast wind or well illuminated by the planetary nebula nucleus. The optical image of multiple shells may unveil the past history of the superwinds better than the SED of the star when it is a dusty AGB star. Nonetheless, these shells must have had their root in the AGB phase.

7. CONCLUSIONS

1. We have successfully modeled the dust shells around oxygen-rich AGB stars with the inclusion of a strong density enhancement in the radial density distribution. This density enhancement is intended to represent the effects of a superwind phase in the mass loss caused by a thermal pulse in the helium-burning shell of the star.

2. The SEDs of two dusty stars with low to moderate optical depths in their shells ($\tau_{9.7} < 3$) in general did not benefit from a superwind model. A conventional r^{-2} density distribution fitted the SEDs of these two stars just as well as our superwind models.

3. The SEDs of three very dusty RLOH/IR stars ($\tau_{9.7} > 3$) are better fitted by our superwind models. The superwind models that best fitted these optically thick dust shells have the density enhancement well out from the star. These models produce more far-infrared emission and deeper 18 μm absorption than conventional models. These models also cover a much wider range in observed *IRAS* 12, 25, and 60 μm colors than is possible with conventional models.

4. Optically thick superwind models with a distant density enhancement present a difficult conceptual problem. Because the density enhancement from a past superwind event has moved well away from the star, its contribution to the total optical depth of the shell is very small. This means that the very dusty OH/IR stars must have very high mass-loss rates independent of a superwind phase that was caused by a thermal pulse.

5. If this past superwind is extrapolated back to times just after the onset of the superwind, extremely high optical depths and very peculiar SEDs are predicted by the models. This early phase for a superwind that begins on top of an already very high mass-loss wind is not observed. It is possible that the combination of the relatively short timescales and high optical depths characteristic of this phase makes stars in the phase difficult to detect.

This study was supported by the Korean Ministry of Education through the Research Fund.

REFERENCES

Balick, B., Gonzaliez, G., Frank, A., & Jacoby, G. 1992, ApJ, 392, 582
Bedijin, P. J. 1987, A&A, 186, 136
Blommaert, J. A. D. L., van der Veen, W. E. C. J., & Habing, H. J. 1993, A&A, 267, 39
Bohren, C. F., & Huffman, D. R. 1983, Absorption and Scattering of Light by Small Particles (New York: Wiley)
Bowen, G. H. 1988, ApJ, 329, 299
Chengalur, J. N., Lewis, B. M., Eder, J., & Terzian, Y. 1993, ApJS, 89, 189
Egan, M. P., Leung, C. M., & Spagna, G. F., Jr. 1988, Comput. Phys. Comm., 48, 271
Evans, N. J., & Beckwith, C. 1977, ApJ, 217, 729
Forrest, W. J., et al. 1978, ApJ, 219, 114
Frank, A., van der Veen, W. E. C. J., & Balick, B. 1994, A&A, 282, 554
Groenewegen, M. A. T. 1994, A&A, 290, 544
Herman, J., & Habing, H. J. 1985, Phys. Rep., 124, 255
Herman, J., Isaacman, R., Sargent, A., & Habing, H. J. 1984, A&A, 139, 171
Iben, I. 1975, ApJ, 196, 525
IRAS Point Source Catalog. 1986, Joint *IRAS* Science Working Group (Washington: GPO)
Jones, T. J. 1987, in The Late Stages of Stellar Evolution, ed. S. Kwok & S. R. Potasch (Dordrecht: Reidel), 1
Jones, T. J., & Gehrz, R. D. 1990, AJ, 100, 274
Jones, T. W., & Merrill, K. M. 1976, ApJ, 209, 509
Kozasa, T., Hasegawa, H., & Seki, J. 1984, Ap&SS, 98, 61
Kwok, S. 1975, ApJ, 198, 583
Le Squeren, A. M., Sivagnanam, P., Dennefeld, M., & David, P. 1992, A&A, 254 133
Lepine, J. R. D., Ortiz, R., & Epchtein, N. 1995, A&A, 299, 453
Ney, E. P., & Merrill, K. M. 1980, Study of Sources in AFGL Rocket Infrared Study (AFGL-TR-80-0050)
Renzini, A. 1981, in Physical Processes in Red Giants, ed. I. Iben & A. Renzini (Dordrecht: Reidel), 431
Rowan-Robinson, M., & Harris, S. 1983, MNRAS, 202, 767
Suh, K. W. 1991, Ap&SS, 181, 237
Suh, K. W., Jones, T. J., & Bowen, G. H. 1990, ApJ, 358, 588
van der Veen, W. E. C. J., Omont, A., Habing, H. J., & Matthews, H. E. 1995, A&A, 295, 445
Vassiladis, E., & Wood, P. R. 1993, ApJ, 413, 641
———. 1988, ApJ, 331, 435
Volk, K., & Kwok, S. 1989, ApJ, 342, 345
Werner, M. W., Beckwith, S., Gatley, I., Sellgren, K., Berriman, G., & Whiting, D. L. 1980, ApJ, 239, 540
Wood, P. R. 1990, in From Miras to Planetary Nebulae: Which Path Evolution, ed. M. O. Minnessier & A. Omont (Gif sur Yvette: Editions Frontières), 67
Xiong, G. Z., Chen, P. S., & Gao, H. 1994, A&AS, 108, 661